Adsorption (2008) 14: 743–754
DOI 10.1007/s10450-008-9123-z

A molecular simulation study of the distribution of cation in zeolites

C. Abrioux · B. Coasne · G. Maurin · F. Henn · A. Boutin · A. Di Lella · C. Nieto-Draghi · A.H. Fuchs

Received: 30 April 2007 / Revised: 21 February 2008 / Accepted: 18 April 2008 / Published online: 8 May 2008

Abstract NVT Monte Carlo simulations are first used to describe the distribution of Na cations in Faujasite for several Si/Al ratios. These calculations were performed by combining two different sets of potential parameters combined with both T-atoms and explicit Si,Al models. Grand Canonical Monte Carlo simulations are then employed to investigate the influence of water adsorption on the distribution of cations in the case of a Faujasite sample with 56 cations (NaY56). These simulations data are compared to available experimental data and the influence of the choice of the forcefield for describing the cation/zeolite interaction on these results is discussed.

Keywords Faujasite · Distribution of cations · Water adsorption · Grand canonical Monte Carlo simulation · Interatomic potential

C. Abrioux · B. Coasne (✉) · G. Maurin · F. Henn
Physicochimie des Matériaux Désordonnés et Poreux, Institut Charles Gerhardt Montpellier, UMR 5253 CNRS, Université Montpellier II, ENSCM, Montpellier, France
e-mail: bcoasne@lpmc.univ-montp2.fr

A. Boutin · A. Di Lella
Laboratoire de Chimie Physique, UMR 8000 CNRS, Université Paris-Sud, Orsay, France

C. Nieto-Draghi
Institut Français du Pétrole, Rueil-Malmaison, France

A.H. Fuchs
Ecole Nationale Supérieure de Chimie de Paris, Paris, France

1 Introduction

Zeolites are microporous materials with pores having a width of a few angstroms (Baerlocher et al. 2001). These systems attract a great deal of attention because of their use in industry for catalysis, phase separation, ionic exchange, ... (Corma 1997; Soler-Illia et al. 2002). The significant impact of zeolites results from the large surface area, the nanoscopic size of the pores, and the large variety of chemical compositions of these materials. From a fundamental point of view, zeolites are model systems that can be used to investigate the effect of nanoconfinement on the thermodynamic and dynamic properties of fluids (Karger et al. 2003; Demontis and Suffritti 1997). Among this class of materials, significant effort has been devoted to deeper understanding the properties of Faujasite zeolites, due to their importance for applications in catalysis and phase separation (alkylation, transalkylation, isomerization of *m*-xylene into *p*-xylene, cracking catalysis, etc.). The substitution of Si by Al atoms in aluminosilicate zeolites such as Faujasite introduces charge defects that are compensated by extra-framework cations (Li^+, Na^+, K^+, ...). Many experimental and theoretical studies have shown that the location of these cations plays a crucial role on the thermodynamics, dynamics, and catalysis of adsorbed molecules (Meunier 2001; Devautour et al. 2001; Moïse et al. 2001; Maurin et al. 2004, 2005; Plant et al. 2006).

Many cation/zeolite interatomic potentials have been implemented in molecular simulations to predict the distribution of cations in zeolite in presence or not of adsorbed molecules (Kramer et al. 1991; Jaramillo and Auerbach 1999; Di Lella et al. 2006; Ramsahye and Bell 2005). These pairwise potential functions include both short-range repulsion and dispersion terms combined with a coulombic contribution between the cation and each atom of the zeolite

framework (Si, O, Al). Molecular simulations used to validate such potentials were performed either for rigid or flexible zeolite framework. In addition, the sets of charges carried by each atom of the system were selected to be consistent with the models used for deriving the parameters of the interatomic potentials. As a result, it makes it difficult to obtain a complete understanding of the validity and transferability of these interatomic potentials required for investigating the behavior of the extra-framework cations in zeolites. The situation is even more puzzling as different models were considered in the previous works mentioned above; some authors used models in which the chemical disorder of the zeolite is treated by introducing Si and Al atoms with different charges (Kramer et al. 1991; Jaramillo and Auerbach 1999), while others considered T-atom models in which the Si and Al atoms are not distinguished (Blake et al. 1998; Buttefey et al. 2001; Beauvais et al. 2004, 2005). The use of T-atoms allows avoiding the tedious task of averaging the results over a large number of (Si, Al) configurations. However, using such an average model cannot capture all the details of the cation/zeolite interaction. Consequently, the T-atom model is rather appropriate when one aims at simulating/predicting macroscopic properties such as the adsorption isotherm and enthalpy of adsorption (Smit and Krishna 2003). On the other hand, an explicit model is usually required to deeper understanding the microscopic mechanisms involved upon adsorption.

The aim of the present paper is to compare the distribution of cations in dehydrated and hydrated Faujasite when the T-atom and the explicit Si/Al models are used. To do that, we selected two cation/zeolite interatomic potentials and we investigated the location of sodium cations in anhydrous Faujasite zeolite with several Si/Al ratios. This work has been motivated by the fact that very few studies have been done to understand the effect of the use of such models (Jaramillo and Auerbach 1999; Mellot-Draznieks et al. 2001). We first report for the T-atom model the distribution of cations among the different crystallographic sites for the whole range of Si/Al ratios. We then investigate for the explicit Si/Al model samples with 56 and 96 cations per unit cell; they correspond to Si/Al ratios of 2.4 (Faujasite NaY56) and 1.0 (Faujasite NaX96), respectively. In the second part of this work, we focus on the Faujasite NaY56 and address the effect of water adsorption on the distribution of cations. Comparison with experimental data is used to discuss the ability of the different interatomic potentials for describing the distribution of cations in Faujasite.

2 Computational details

2.1 Faujasite zeolite

Faujasite is an aluminosilicate zeolite of general chemical formula $M_{x/m}$, Al_x, Si_{192-x}, O_{384}, where M is a cation of charge $+m$ (Meier and Olson 1978). The number x of cations in the unit cell can vary from 0 up to 96, depending on the Si/Al ratio. The crystalline structure of Faujasite as well as the position of the extra-framework cation can be extracted from X-ray or Neutron diffraction (Fitch et al. 1986; Vitale et al. 1997; Mellot 1993). The Faujasite structure belongs to the *Fd3m* space group of symmetry with a unit cell of 24.8536 Å that contains 192 TO_4 tetrahedra (with T = Si or Al). The extra-framework cations in Faujasite are located in different crystallographic sites that are usually labelled using roman numbers (Fig. 1). The sites I are located in the centre of the hexagonal prism, while sites I′ are present in the sodalite cage towards the hexagonal prism. Sites II and Sites III′ are located in the 6-ring and 12-ring windows of the supercage respectively. The position of the sites IV and V (not shown here) are in the centre of the supercage and of the 12-member rings, respectively.

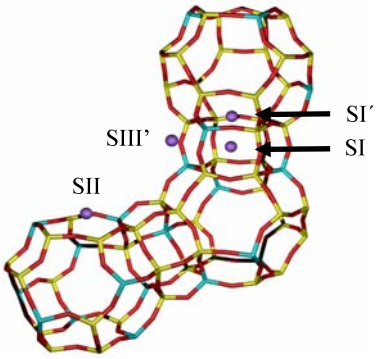

Fig. 1 Molecular graphic representing the Faujasite type zeolites structure with three sodalite cages connected by two hexagonal prisms and describing the main crystallographic sites (SI, SI′, SII and SIII′) for the extra-framework cations

In this work, we decided to consider a rigid framework. As far as thermodynamic properties are concerned, it can be reasonably assumed that the flexibility of zeolite is important only when the size of the adsorbate is similar to those of the windows (Demontis and Suffritti 1997). In our case, water molecules are small enough to pass through the 6-rings to reach both the sodalites and the supercages of Faujasite without considering the flexibility of the framework. As a consequence, calculations of the adsorption properties taking into account only the mobility of the extra-framework cations is reasonable, as attested by several papers in this field (Calero et al. 2004; Beauvais et al. 2004, 2005) which reproduce reasonably experimental data.

2.2 Interatomic potentials

Two pairwise potentials were considered in this work to model the interaction between the sodium cations and the zeolite framework: the potential reported by Di Lella et al. (2006) and the potential developed by Kramer et al. (1991).

In what follows, these two potentials will be referred to as potential 1 and potential 2, respectively. Both interaction potentials consist of a Buckingham potential and a coulombic contribution:

$$U_{\mathrm{NaO_z}} = A_{\mathrm{NaO_z}} \exp(-B_{\mathrm{NaO_z}} r_{\mathrm{NaO_z}}) - \frac{C_{\mathrm{NaO_z}}}{r^6_{\mathrm{NaO_z}}} + \frac{q_{\mathrm{Na}} q_{\mathrm{O_z}}}{r_{\mathrm{NaO_z}}} \quad (1)$$

Where $A_{\mathrm{NaO_z}}$, $B_{\mathrm{NaO_z}}$, and $C_{\mathrm{NaO_z}}$ correspond to the Buckingham potential parameters for the interaction between the Na cation and the oxygen atom of the zeolite $\mathrm{O_z}$. q_{Na} and $q_{\mathrm{O_z}}$ are the charges carried by Na and $\mathrm{O_z}$. The cations/cations (Na/Na, Na/Si, and Na/Al) interactions are treated only as a coulombic contribution. For each potential, two models for describing the framework are considered: a "T-atom" version that attributes the same charge for Si and Al and an "explicit" version that distinguishes the Al and Si atoms. For the explicit model, the simulations were performed for a number of different (Si,Al) configurations large enough to get results that are independent of any particular realization of the zeolite framework. In this way, at least 5 configurations were built by randomly distributing the x Al atoms among the 192 possible T-sites and obeying to the Lowenstein's rule, which states that two Al atoms cannot be connected to the same $\mathrm{O_z}$ atom (Loewenstein 1954). Furthemore, in order to evaluate the effect of the partition of the aluminium atoms on the distribution of cations, we prepared a "pathological" configuration in which all the Al atoms are located on the left side of the x-axis of the Faujasite unit cell.

Potential by Di Lella et al. (potential 1) This forcefield was previously introduced by Di Lella et al. for modeling the distribution of cations in Faujasite (NaY52 and NaX76) (Di Lella et al. 2006). It corresponds to a Buckingham potential with the parameters proposed by Jaramillo and Auerbach (1999). The charges used for this potential are interpolated from the charges calculated by Uytterhoeven *et al.* using the Electronegativity Equalization Method for Faujasite with 48 and 96 Al atoms (Uytterhoeven et al. 1992). In the initial T-atom version of this potential, the charge q_T on the T-atom model was determined for a Faujasite sample with x Al atoms from the following electroneutrality condition:

$$192 q_T + 384 q_{\mathrm{O_z}}(x) + x q_{\mathrm{Na}} = 0 \quad (2)$$

Using this parameterization, the charges on the O and T atoms are -0.8273 and 1.363 respectively for the NaY56 and -0.85 and 1.2 respectively for the NaX96. In the case of the explicit model, we used the same method with the charges for the Si, Al, and O atoms from the paper by Uytterhoeven *et al.* This ensures that the same charge is used for the O atoms between the T-atom and explicit models.

Potential by Kramer et al. (potential 2) These authors derived a force field for silicas, aluminophosphates, and zeolites by combining *ab-initio* calculations and fit on experimental data for the structure of α-quartz (Kramer et al. 1991). This interatomic potential is the sum of a Buckingham potential and the coulombic contribution. The charge of $q_{\mathrm{O_z}}, q_{\mathrm{Si}}$, and q_{Al} in the case of the explicit model are $-1.2\mathrm{e}^-$, $2.4\mathrm{e}^-$, and $1.4\mathrm{e}^-$ respectively. In contrast, when using this interatomic potential with the T-atom model, the charge of the oxygen atoms remains the same and those of the T atom, which depends on the number of cations ($q_{\mathrm{Na}} = 1.0\mathrm{e}^-$), is fixed at a value that ensures the electroneutrality of the zeolite sample.

In order to study water adsorption in Faujasite, the TIP4P model for the water molecules (Jorgensen et al. 1983). This model is based on a description of the water molecule using 4 sites; 3 electrostatic centres (the 2 H atoms with a charge of $q = 0.52\mathrm{e}^-$ and 1 "pseudo-atom" with a charge of $q = -1.04\mathrm{e}^-$), and one repulsion-dispersion centre located on the O atom. The interaction of the water molecules with the zeolite framework is described as the sum of a coulombic contribution and a Lennard-Jones interaction between the oxygen atom $\mathrm{O_w}$ of the water molecule and the oxygen atom $\mathrm{O_z}$ of the zeolite. The sodium cation–water LJ interaction parameters were borrowed from the work of Dang (1995).

2.3 Monte Carlo techniques

Canonical Monte Carlo (NVT). The distribution of sodium cations in all of the Faujasites were simulated at $T = 300$ K using NVT Monte Carlo (MC) simulations. The simulations were carried out using both the GIBBS code developed by the Institut Français du Pétrole and Centre National de la Recherche Scientifique (Orsay) and a "home-made" code developed in Montpellier. Following the work by Di Lella et al. (2006), random translations were attempted with a maximum displacement of 0.3 Å in order to obtain an acceptance probability of 40–50%. We also used MC steps that consist of simultaneous deletion/insertion of a particle as originally proposed by the same authors (Di Lella et al. 2006). This motion can be seen as a super-displacement of a randomly selected particle through the entire simulation box, which significantly improves the sampling of phase space. The acceptance probability for such moves in the frame of the Metropolis sampling algorithm is equal to that of classical displacements as the number of cations is kept constant. The simultaneous deletion/insertion of particles has proven to be very efficient in simulating the effect of water adsorption on the distribution of cations in zeolites (Di Lella et al. 2006). Starting with a random initial configuration of the x cations, the system is allowed to equilibrate for 80×10^6 MC Steps (a MC step being either a cation displacement or

a simultaneous cation deletion/insertion). Then the data "at equilibrium" were averaged for another 80×10^6 MC Steps. Ewald sums were used to calculate the coulombic terms. The parameters for the Ewald sum were $\alpha = 2.5$ and $k_{max} = 10$.

Grand Canonical Monte Carlo (μVT). The adsorption of water in Faujasite was simulated at $T = 300$ K using Grand Canonical Monte Carlo simulations (GCMC). The GCMC technique is a stochastic method that simulates a system having a constant volume V (the pore with the adsorbed phase), in equilibrium with an infinite reservoir of particles imposing its chemical potential μ and temperature T (Nicholson and Parsonage 1982; Allen and Tildesley 1987; Frenkel and Smit 2002). The absolute adsorption isotherm is given by the ensemble average of the number of adsorbed molecules as a function of the pressure of the gas reservoir P (the latter is obtained from the chemical potential μ according to the bulk equation of state for an ideal gas). The isosteric heat adsorption is given from fluctuations over the energy and number of adsorbed molecules (Nicholson and Parsonage 1982). As for the simulations without adsorbed water molecules, Ewald sums were used to calculate the coulombic term and periodic boundary conditions were used along the 3 directions x, y, and z. The parameters for the Ewald sums were the same as those used for the dehydrated zeolites.

3 Results and discussion

3.1 Dehydrated Faujasite

3.1.1 Potential by Di Lella et al. (potential 1)

T-atom model Figure 2 reports the distribution of the extra-framework cations in the 4 different sites (I, I′, II, III′) of the dehydrated Faujasite as a function of the number x of cations. For $x = 48$ (NaY48), the distribution of cations is 16 cations in site I, 0 cations in site I′, 32 cations in site II, and 0 in site III′. We summarize this result using the condensed form (16, 0, 32, 0). All of the sites I and II are occupied for this Faujasite sample NaY48. The number of cations in site II remains constant as the total number of cations increases from $x = 48$ up to $x = 96$. This result shows that site II corresponds to the most stable site, in agreement with previous molecular simulation results (Di Lella et al. 2006). In addition, the higher stability of cations in site II is consistent with recent dielectric relaxation spectroscopy (DRS) measurements for NaY56 (Nicolas et al. 2008a, 2008b); the energy barrier required to de-trap the cations was found to be higher for site II than for sites I and I′, which means that the stability sequence for these cations sites are the following: E(II)>E(I)>E(I′). This trend can be explained by geometric considerations based on the interatomic distances between cation in each site and its surrounding oxygen atoms

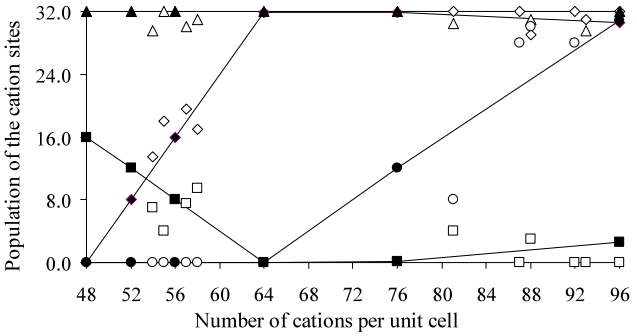

Fig. 2 Distribution of sodium cations in the 4 sites of the dehydrated Faujasite as a function of the number of cation per unit cell: (*squares*) site I, (*diamonds*) site I′, (*triangles*) site II, (*circles*) site III′. These results were obtained using the potential 1 for the T-atom model. Simulation data correspond to the *filled symbols* connected by *solid lines*, while experimental data correspond to the *empty symbols* (Jiràk et al. 1980; Olson 1995; Vitale et al. 1997; Zhu and Seff 1999; Porcher et al. 1999)

of the zeolite framework. As the total number of cations increases from 48 to 64, the cations in site I leave this site to occupy site I′. This inversion between sites I and I′ can be explained as follows. For $x = 48$, all of the sites I are occupied by cations. When x increases, the cations start filling sites I′. The short distance between sites I and I′, i.e. 2.18 Å, leads to a strong coulombic repulsion between cations in these two sites. Consequently, it is preferable to decrease the number of cations in site I and favor the occupation of the sites I′. When all of the sites I′ are filled ($x = 64$), the cations start filling the sites III′. As can be observed in Fig. 2, these results reproduce the experimental trend reported in the literature (Jiràk et al. 1980; Olson 1995; Vitale et al. 1997; Zhu and Seff 1999; Porcher et al. 1999).

Explicit model (Si,Al) Table 1 reports the distribution of cations among the 4 sites in the sample NaY56 for 5 different (Si,Al) configurations of the framework. We also compare the mean distribution of cations for these 5 configurations with those obtained for the pathological configuration (see Sect. 2.2). There is no obvious difference between the distribution of cations for the pathological model and that obtained by averaging over the 5 (Si,Al) configurations. This result shows that the distribution of cations for this particular Faujasite with 56 cations is not very sensitive to the degree of homogeneity of the location of the Al atoms in the zeolite framework. We also report in Table 1 the results obtained above for the T-atom model. There is no drastic difference between the results for the T-atom model and those for the (Si,Al) model as the data fall within the error bar. This result is due to the fact that the charge difference between the Si and Al atoms is rather small ($\Delta q \sim 0.2e^-$). As a result, the use of a T-atom model for this potential is a reasonable approximation as the Si and Al atoms have similar properties. We corroborated this result by performing

Table 1 Distribution of sodium cations in the 4 sites of Faujasite NaY56 for 5 different (Si,Al) configurations of the framework. The data reported in bold are the average distribution out of the 5 configurations. These results were obtained using the potential 1 coupled with the explicit model. The data in italic are those obtained for the pathological configuration (see text). The results obtained for the T-atom model with the potential 1 are also provided

Configuration	Site I	Site I′	Site II	Site III′
1	8.06	15.94	32.00	0.00
2	9.99	12.01	32.00	2.00
3	10.00	12.00	32.00	2.00
4	11.00	10.00	32.00	3.00
5	12.00	8.00	32.00	4.00
Explicit (Si,Al)	**10.21**	**12.59**	**32.00**	**2.20**
Pathological (Si,Al)	*10.02*	*11.98*	*32.00*	*2.00*
T-atom	8.00	16.00	32.00	0.00

Table 2 Distribution of sodium cations in the 4 sites of Faujasite NaX96. These results were obtained using the potential 1 for both the T-atom and explicit models

	Site I	Site I′	Site II	Site III′
Explicit (Si,Al)	**0.10**	**31.90**	**32.00**	**32.00**
T-atom	2.57	30.62	32.00	30.81

calculations (results not reported here) for the same potential with larger charge differences between the Si and Al atoms; we found that when the charge difference becomes larger ($\Delta q = 1.0e^-$), the distribution of cations for the explicit model significantly differs from that obtained for the T-atom model.

Table 2 compares the distribution of cations among the 4 sites in NaX96 for the explicit model and the T-atom model. For this Faujasite sample, there is only one possible partition of the Al atoms (given that the configuration must obey the Lowenstein's rule). As for the Faujasite NaY56, we found that the difference between the distribution of cations for the T-atom model and that for the explicit model is not significant. Again, this result is due to the small charge difference between the Si and Al atoms using this potential. In addition, for this system in which one over two T-atoms is an Al atom, the Al configuration provides an average picture of the Faujasite zeolite close to that corresponding to the T-atom model.

3.1.2 Potential by Kramer et al. (potential 2)

T-atom model Figure 3 shows the distribution of cations in the 4 sites (I, I′, II, III′) of the dehydrated Faujasite as a function of the number of cations for the T-atom model. For $x = 48$, the distribution of cations is (0, 16, 32, 0). Each site II and half of the sites I′ are occupied by a cation for

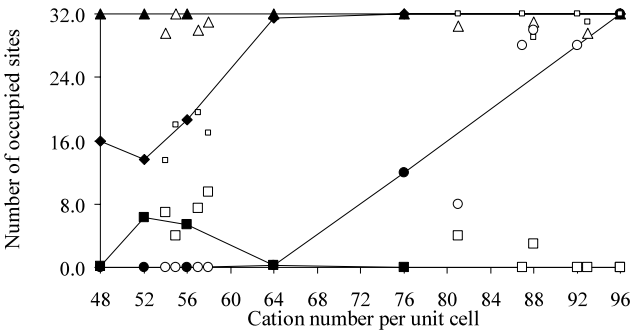

Fig. 3 Distribution of sodium cations in the 4 sites of the dehydrated Faujasite as a function of the cation number per unit cell: (*squares*) site I, (*diamonds*) site I′, (*triangles*) site II, (*circles*) site III′. These results were obtained using the potential 2 for the T-atom model. Simulation data correspond to the *filled symbols* connected by *solid lines*, while experimental data correspond to the *empty symbols* (Jiràk et al. 1980; Olson 1995; Vitale et al. 1997; Zhu and Seff 1999; Porcher et al. 1999)

this particular Faujasite. The number of cations in site II remains constant as the total number of cations increases. As found for potential 1, this result suggests that site II corresponds to the most stable site. As x increases from 48 up to 64, a non monotonous behavior for the population of site I and I′ is observed. From $x = 48$ to 52, the population of site I′ decreases while that of site I increases. In contrast, from $x = 52$ to 64, the cations move from site I to site I′. When every site I′ is filled ($x = 64$), the cations start filling the sites III′. The main difference between the distributions obtained with potentials 1 and 2 is observed for the sample NaY48; potential 1 predicts that all of the sites I are filled while potential 2 leads to the occupation of sites I′. To understand the origin of this difference, we calculated the energy profile for one cation along the axis ⟨111⟩ (results not reported). The crystallographic positions of the sites I, I′, and II are located on this axis. We included in these calculations both the repulsion-dispersion and electrostatic contributions. Site II is found to be the most stable site for both potentials 1 and 2, which is consistent with our simulation data reported above. For both potentials 1 and 2, it is also found that site I′ is more favorable than site I. This result explains why sites I′ are filled prior to sites I when potential 2 is used. In contrast, this result does not explain why site I are filled prior to sites I′ when potential 1 is used. This is probably due to the fact that energy profile calculations are performed for a single cation, which does not include cation/cation repulsion. The latter contribution, which is known to be significant, may invert the relative stability of sites I and I′ when several cations are present in the system.

We also report in Fig. 3 the experimental distribution of cations reported in the literature (Jiràk et al. 1980; Olson 1995; Vitale et al. 1997; Zhu and Seff 1999; Porcher et al. 1999). As for the results obtained with potential 1, the data for potential 2 are found to reproduce in a reasonable way

Table 3 Distribution of sodium cations in the 4 sites of Faujasite NaY56 for 5 different (Si,Al) configurations of the framework. The data in bold are the average distribution out of the 5 configurations. These results were obtained using the potential 2 for the explicit model. The data in italic are those obtained for the pathological configuration (see text). The results obtained for the T-atom model with the potential 2 are also provided

Configuration	Site I	Site I′	Site II	Site III′
1	2.23	19.73	24.70	9.35
2	1.01	20.99	24.48	9.53
3	2.13	17.96	29.06	6.85
4	3.46	20.54	25.04	6.96
5	2.06	18.94	28.41	6.59
Explicit (Si,Al)	**2.18**	**19.63**	**26.34**	**7.86**
Pathological (Si,Al)	*0.00*	*18.00*	*23.00*	*15.00*
T-atom	5.40	18.60	32.00	0.00

the experimental trend. Given the dispersion of the experimental results, we cannot conclude on which interatomic potential is the most suitable to describe the distribution of cations in zeolites. Even the large difference between the simulated data for potentials 1 and 2 in the case of NaY48 and NaY52 cannot be used to decide on the validity of these potentials, due to the lack of experiments for such samples.

Explicit model (*Si,Al*) Table 3 shows the distribution of cations in the 4 different sites in Faujasite NaY56 for 5 (Si,Al) configurations of the zeolite framework. The average distribution over the 5 configurations is compared with those obtained for both the pathological configuration and the T-atom model. A significant deviation is observed between the data for the averaged explicit model and those for the T-atom model. This difference between the two models is more pronounced than that previously reported for potential 1. This result is due to the large charge difference ($\Delta q = 1.0e^-$) between the Si and Al atoms for potential 2. The significant difference (in particular for the sites III′) is also observed between the data for the pathological configuration and those for the average distribution. This result shows that the distribution of cations for potential 2 is sensitive to the degree of homogeneity of the partition of the Al atoms in the zeolite framework, due to the large charge difference for this potential. Table 4 compares the distribution of cations in the 4 sites of Faujasite NaX96 for both the explicit and the T-atom models. For this particular sample, the simulations for the T-atom model give the same results as those obtained with the explicit model. As mentioned above, this result is due to the fact that there is only one possible configuration for the Al atoms in the zeolite framework for this sample.

Table 4 Distribution of sodium cations in the 4 sites of Faujasite NaX96. These results were obtained using the potential 2 for both the T-atom and explicit models

	Site I	Site I′	Site II	Site III′
Explicit (Si,Al)	**0.00**	**32.00**	**32.00**	**32.00**
T-atom	0.00	32.00	32.00	32.00

3.2 Hydrated Faujasite

In this section, we investigate the effect of water adsorption on the distribution of cations in the Faujasite NaY56 using the interatomic potentials 1 and 2. In this preliminary work, each potential is used within the frame of the model (T-atom versus explicit) for which it was derived. For instance, potential 1 is used with the T-atom model (as treated in the recent study by Di Lella et al. 2006) while potential 2 is implemented with its original explicit (Si,Al) model (Kramer et al. 1991). Figure 4a shows the water adsorption isotherm at 300 K in Faujasite NaY56 obtained using the two interatomic potentials. These simulated data are also compared to the experimental measurements obtained by both Boddenberg *et al.* for the Faujasite NaY56 (Boddenberg et al. 2002) and Paulin and Bellat for the Faujasite NaY52 (Paulin and Bellat 2008). We also report the data for the NaY52 as they are very close to the data for the NaY56. At low pressure, the adsorbed amount sharply increases with pressure for both potentials. The slope of the adsorption isotherm for potential 2 is larger than that for potential 1. In addition, potential 2 leads to a saturation capacity ($\sim$ 290 water molecules) which is larger than that for potential 1 ($\sim$ 250 water molecules). The data for potential 1 are in better agreement with the experiments than those for potential 2. This result suggests that the largest saturation capacity and slope of the adsorption isotherm with potential 2 is due to a too large H_2O/zeolite affinity for this potential.

Figure 4b shows the isosteric heat of adsorption (Qst) as a function of the water loading. We also report the experimental data by Boddenberg et al. (2002). As expected for a system with a heterogeneous surface, Qst first decreases with increasing the number of adsorbed water molecules, and then remains constant. The large fluctuations in the Qst curve at high loadings are due to poor statistics in this range (the error being large when the fluctuations over the number of water molecules are small). However, it can be seen that Qst is always larger at high loading than the heat of liquefaction of water ($\sim$ 44 kJ·mol^{-1}), which indicates that the water molecules always feel the electric field of the zeolite surface even at large adsorbed amounts. The Qst obtained with potential 1 decreases from 80 kJ·mol^{-1} down to 60 kJ·mol^{-1} when the loading increases from 0 up to $\sim$ 60 H_2O/u.c., while it decreases for potential 2 from 100 to 65 kJ·mol^{-1} when the loading increases from 0 up

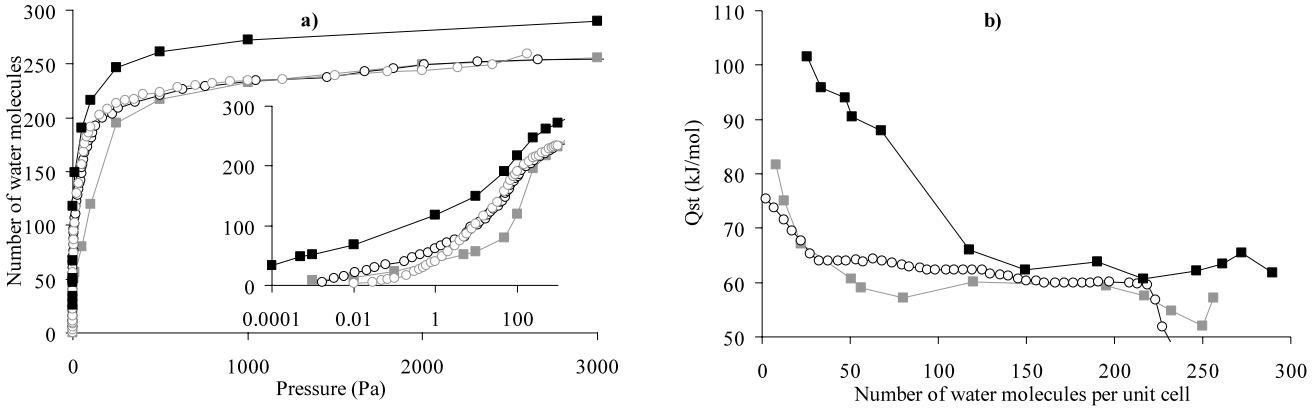

Fig. 4 (**a**) Absolute isotherms for water and (**b**) Isosteric heat adsorption (Qst) as a function of loading for NaY56 at 300 K. These results were obtained using the potential 1 with T-atom model (*grey solid line*), and potential 2 with the explicit model (Si,Al) (*black solid line*). The *empty black symbols* are the experimental data by Boddenberg et al. for NaY56 while the *empty grey symbols* are the experimental data provided by Paulin and Bellat for NaY52. *Inset* in (**a**): same data plotted using a logarithmic scale in the low range pressure [0–1000 Pa]

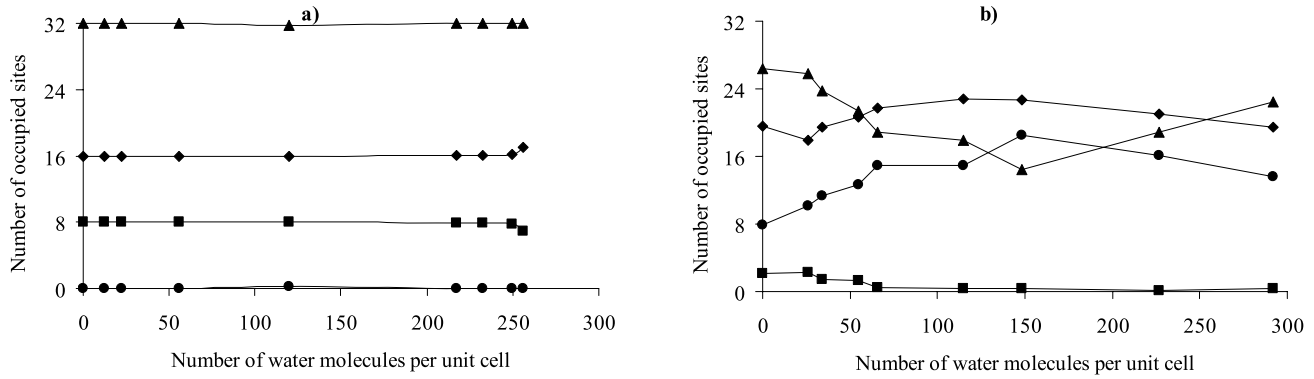

Fig. 5 Distribution of sodium cations in the 4 sites of the hydrated Faujasite NaY56 as a function of the number of adsorbed water molecules per unit cell: (*squares*) site I, (*diamonds*) site I′, (*triangles*) site II, (*circles*) site III′. These results were obtained (**a**) using the potential 1 with T-atom model and (**b**) using potential 2 with the explicit model (Si,Al)

to ~ 120 H_2O/u.c. The largest Qst for potential 2 is consistent with the highest slope of the adsorption isotherm at low loading observed when this potential is employed (Fig. 4a). On the other hand, the experimental Qst value decreases from 75 kJ·mol^{-1} at zero loading down to 65 kJ·mol^{-1} when 32 water molecules are adsorbed and then remain almost constant whatever the loading. Boddenberg et al. (2002) proposed that the range of loading [0,32 H_2O/u.c.] corresponds to the filling of the sodalite cages, prior to that of the supercages at higher loadings. The loading where a change in the slope of the Qst curve is observed corresponds to ~ 50 and 120 H_2O/u.c. for potentials 1 and 2, respectively. These values overestimate the experimental loading where such a change is observed (~ 32 H_2O/u.c.). We note that potential 1 leads to a better agreement with the experimental values, which is consistent with our previous conclusion.

Figure 5a shows the distribution of cations obtained using potential 1 for NaY56 as a function of the number of adsorbed water molecules. Even when water molecules are adsorbed, the cations remain close to the framework (sites I, I′, II, and III′) so that sites IV and V (located at the centre of the supercage and the 12-membered rings, respectively) remain unoccupied. The distribution of cations is close to that obtained for the dehydrated sample (12, 8, 32, 0) in the whole range of loadings. This result significantly differs from those reported in a previous work (Di Lella et al. 2006), in which the distribution of sodium cations for NaY52 and NaX76 was found to be significantly affected by water adsorption. These authors found that: (1) cations in site I are displaced to site I′ for NaY52 while (2) cations in sites I′ are displaced to sites I for NaX76. In both cases, the population in site I′ tends to converge towards a value between 16 (NaY52) and 26 (NaX76). Our results suggest that NaY56 corresponds to an intermediate situation in which the number of cations in

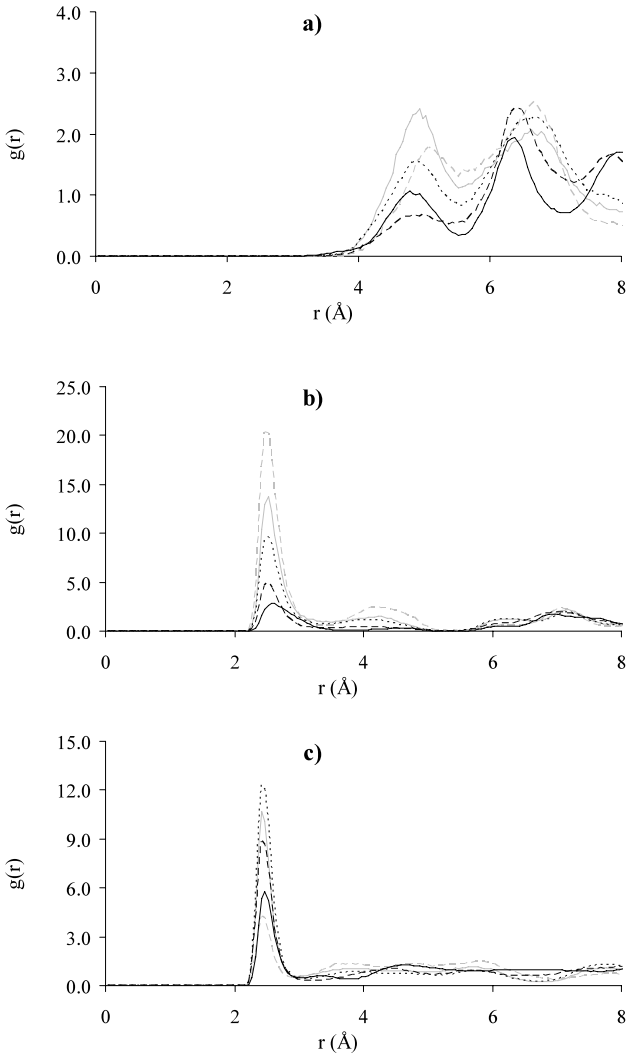

Fig. 6 Pair correlation function $g(r)$ in NaY56 for O_w-Na^+ located in (**a**) site I, (**b**) site I′, (**c**) site II: (*grey dashed line*) 20 molecules adsorbed, (*grey solid line*) 32 molecules adsorbed, (*black dotted line*) 50 molecules adsorbed, (*black dashed line*) 100 molecules adsorbed and (*black solid line*) 250 molecules adsorbed. These results were obtained using the potential 1 with T-atom model

site I′ ($\sim$ 16) has already converged. As a result, the distribution of cations for this particular sample is not affected by water adsorption.

Figure 5b shows the distribution of cations obtained using potential 2 for NaY56 as a function of the number of adsorbed water molecules. This distribution corresponds to the average results over 5 Si/Al configurations. In contrast to the results obtained for potential 1, the distribution of cations is affected by water adsorption for potential 2. As the water loading increases up to 150 water molecules per unit cell, the occupancy of site II decreases whereas that of site III′ increases. This result suggests that the water molecules interact with cations in site II and tend to displace them in the neighbouring sites III′. On the other hand, at high loading, such an effect is reverted; cations in sites III′ are de-trapped to occupy their former position in site II. It has to be emphasized that the number of cations in sites I and I′ is less affected by water adsorption than sites II and III′. These results for potential 2 (Fig. 5b) are in better agreement with experimental data recently obtained with DRS measurements (Nicolas et al. 2008a, 2008b), which showed a significant redistribution of cations upon water adsorption.

To provide a possible microscopic mechanism for water adsorption in the Faujasite NaY56, we report in Fig. 6 the (O_w-Na) pair correlation function obtained when potential 1 is used. We show the contributions for cations located in the different sites I, I′, II. The peak at $\sim$ 2.5 Å for the sites I′ and II corresponds to the typical distance between the oxygen of water molecules and sodium cations. This peak for cations in sites I′ and II is already present when 20 water molecules are adsorbed, which means that the first adsorbed water molecules interact with both sites. We note that the location of such a peak is very similar to that obtained for bare sodium cations in water (Tuñon et al. 1995). In contrast to cations in site I′ and II, the pair correlation function for O_w-Na in site I does not exhibit such a peak, which indicates that the water molecules do not enter the hexagonal prism due to steric hindrance effects.

Figure 7 shows the pair correlation function for O_w-Na located in the different sites as obtained using potential 2. Very similar results are obtained when compared with those extracted by potential 1. For instance, no correlation peak at $\sim$ 2.5 Å is observed between the cations in site I and water. The correlation peak at $\sim$ 2.5 Å for the cations in sites I′ and II appear at loading of 26 and 34, respectively. This result is in full agreement with various experimental findings including microcalorimetry (Boddenberg et al. 2002) and both ^{23}Na and Xe NMR spectroscopy (Hu and Hwang 1998; Gedeon et al. 1988), which clearly demonstrate that the 32 first water molecules are only interacting with the cations in the sodalite cages.

Typical molecular configurations of water adsorbed in NaY56 are provided in Fig. 8 for illustrating the results presented in Fig. 7. We selected these molecular configurations for potential 2 as they show the first water molecules penetrating the sodalite cages, in agreement with experimental data by Boddenberg et al. (2002). The snapshot reported in Fig. 8a shows a typical configuration at low and intermediate loading where the first water molecules significantly displace the cation in site I′ from its original position towards the sodalite cage. Figure 8b shows a configuration which illustrates the hydration process in the supercage above 34 H_2O/u.c. It can be seen that the cation initially in site II can be either slightly displaced from its original crystallographic position (cation represented in green) or moved to a neighbouring sites III′ (cation represented in light blue). This molecular configuration also shows that for this given

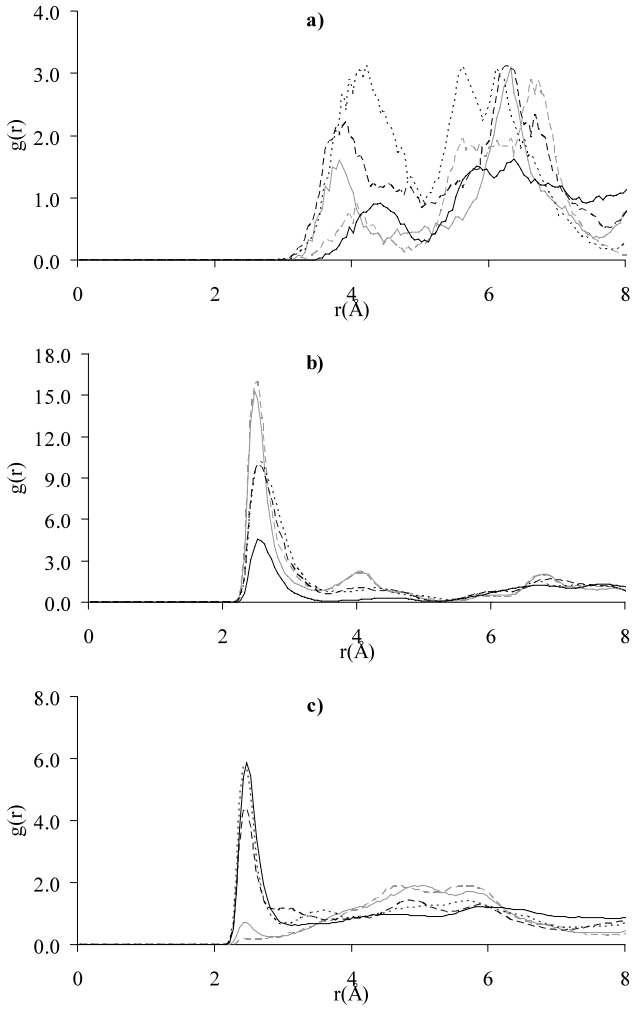

Fig. 7 Pair correlation function $g(r)$ in NaY56 for O_w-Na^+ located in (**a**) site I, (**b**) site I′, (**c**) site II: (*grey dashed line*) 26 molecules adsorbed, (*grey solid line*) 34 molecules adsorbed, (*black dotted line*) 51 molecules adsorbed, (*black dashed line*) 68 molecules adsorbed and (*black solid line*) 247 molecules adsorbed. These results were obtained using the potential 2 with the explicit model (Si,Al)

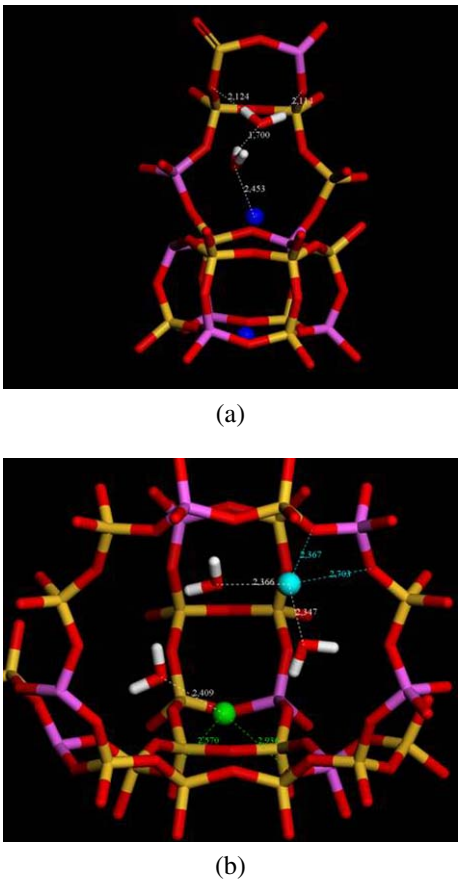

Fig. 8 (Color online) Snapshot of the Faujasite NaY56 obtained using the potential 2. It represents (**a**) hydration of the cation in the sodalite cage for 51 water molecules adsorbed, (**b**) the hydration of cations in sites II in the supercage for 34 water molecules adsorbed. The *green* cation corresponds to a cation which located in a site II, while the *light blue* corresponds to a cation located in a site III′. The rigid framework is represented by colors *yellow* (Si), *pink* (Al) and *red* (O)

loading, a cation located in a site III′ can be solvated by up to 2 water molecules.

Figure 9 shows the pair correlation function between (a) the hydrogen and oxygen of water (H_w-O_w) and (b) the hydrogen of water and oxygen of zeolite (H_w-O_z) calculated using the potential 1. Both pair correlation functions exhibit a characteristic peak around 1.9 Å whatever the loading. As expected, such hydrogen bonding becomes more pronounced as the loading increases due to the increase in the density of adsorbed water molecules. It is also observed that these peaks are only slightly shifted from those for bulk liquid water (Jorgensen and Jenson 1998), which indicates that the zeolite framework does not affect too much the hydrogen bonding between water molecules.

Figure 10 shows the pair correlation function for H_w-O_w (a) and H_w-O_z (b) obtained when potential 2 is used. Again, both pair correlation functions exhibit a peak around 1.9 Å, which shows the formation of hydrogen bonding between the adsorbed water molecules. Such a peak is observed for all loadings, which suggests that hydrogen bonding occurs even when very few water molecules are adsorbed. Similarly, as for potential 1, the hydrogen bonding H_w-O_z with the zeolite framework is also observed as the number of adsorbed water molecules increases.

A typical configuration of the arrangement of 247 water molecules adsorbed in the Faujasite NaY56 is shown in Fig. 11. Two types of molecular organisation can be observed: a) formation of cycles consisting of 4 or 5 water molecules centred around a cation in site II or III′ and b) nearly linear chains of water molecules (a chain of 7 molecules is seen in Fig. 11). Such arrangements are similar to those observed in the bulk liquid phase, in which the molecules tend to form rings and/or chains with an average of 3.6 hydrogen bonds per molecule (Jorgensen and Jenson 1998). Our results show that the water molecules are orga-

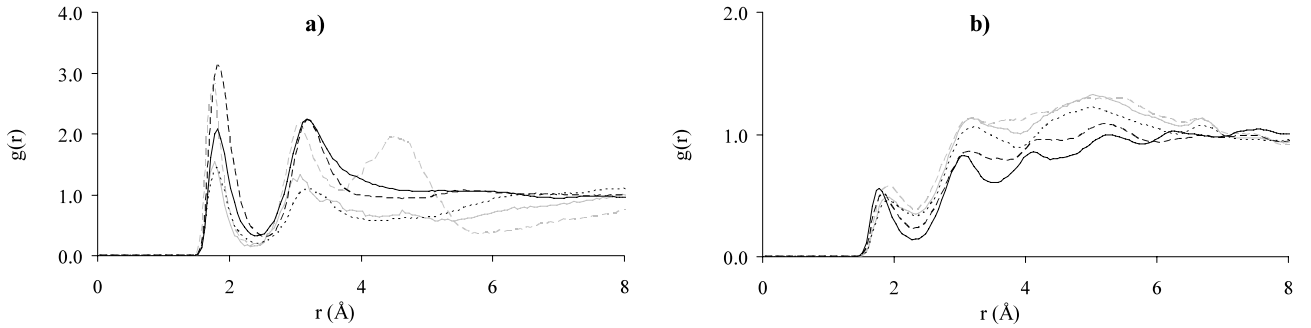

Fig. 9 Pair correlation function $g(r)$ in NaY56 for (**a**) H_w-O_w and (**b**) H_w-O_z: (*grey dashed line*) 20 molecules adsorbed, (*grey solid line*) 32 molecules adsorbed, (*black dotted line*) 50 molecules adsorbed, (*black dashed line*) 100 molecules adsorbed and (*black solid line*) 250 molecules adsorbed. These results were obtained using the potential 1

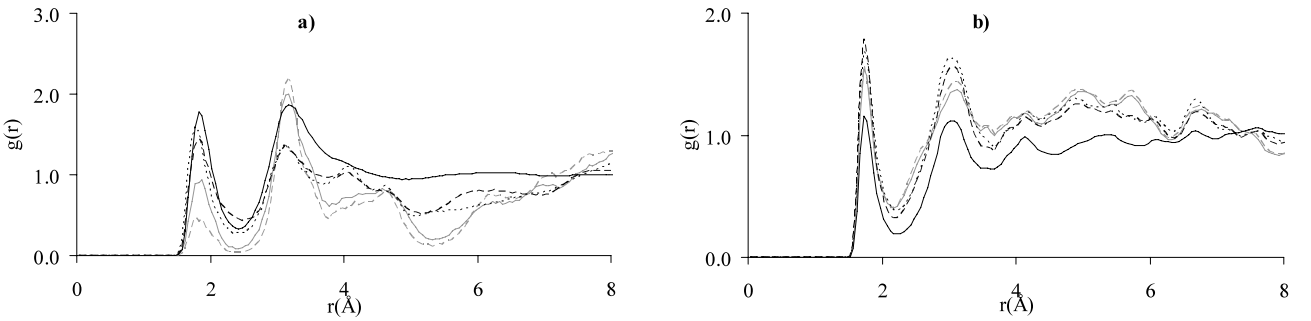

Fig. 10 Pair correlation function $g(r)$ in NaY56 for (**a**) H_w-O_w and (**b**) H_w-O_z: (*grey dashed line*) 26 molecules adsorbed, (*grey solid line*) 34 molecules adsorbed, (*black dotted line*) 51 molecules adsorbed, (*black dashed line*) 68 molecules adsorbed and (*black solid line*) 247 molecules adsorbed. These results were obtained using the potential 2

nized in a bulk-like fashion in the zeolite cavities, although they are in a confined environment.

4 Conclusion

This work reports Monte Carlo simulations on the distribution of sodium cations in Faujasite. Two different types of interatomic potentials are used to describe the interactions between the cations and the zeolite framework: (i) a T-atom model in which the Si and Al atoms are not distinguished and (ii) an explicit model which accounts for the charge difference between the Si and Al atoms. We also address the effect of water adsorption on the distribution of cations and discuss the adsorption mechanisms by calculating pair correlation functions.

Our results for dehydrated Faujasites show that the distribution of cations upon the different crystallographic sites strongly depends on the Si/Al ratio of the Faujasite system. Both results obtained with the potential by Di Lella et al. (2006) and those with the potential by Kramer et al. (1991) are found to reproduce in a reasonable way the trend observed in the experimental data. As a result, we cannot con-

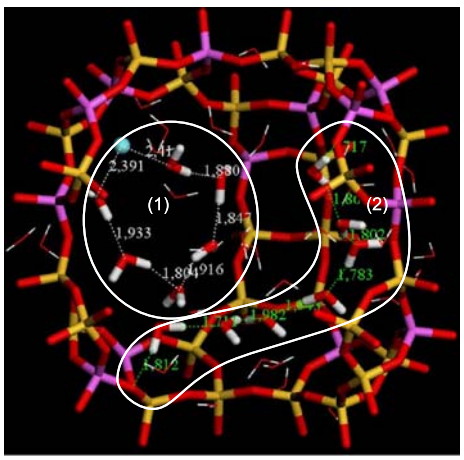

Fig. 11 (Color online) Snapshot of the Faujasite NaY56 loaded by 247 water molecules obtained using the potential 2. This figure depicts the arrangement of the water molecules within the supercage of the Faujasite with (1) characteristic rings or (2) quasi-linear chains. The atoms of the rigid framework are represented using the following colors: *yellow* (Si), *pink* (Al) and *red* (O)

clude on which interatomic potential is the most suitable to describe the distribution of cations in dehydrated zeolites.

Our study on water adsorption in Faujasite NaY56 shows that the choice of the model to describe the zeolite framework (explicit or T-atom) must be guided by the properties under investigation (adsorption isotherm, isosteric heat of adsorption, and distribution of cations). In fact, both models predict similar qualitative results when it comes to thermodynamic data. In contrast, these two models give different results as far as microscopic data are concerned (location of the cations and their redistribution upon water adsorption). Our results for the explicit model suggest that the water molecules are first adsorbed in the sodalite cages and then in the supercages, in qualitative agreement with the experiments by Boddenberg et al. (2002). In contrast, the T-atom model predicts that the water molecules are adsorbed in both cages at low loading. It should be noted that only a potential used with an explicit model (such as potential 2 in the present work) can capture all the details of the microscopic adsorption mechanisms, which can be used to interpret the experimental data collected by different techniques (DRS, NMR spectroscopy). Finally, these results show that two potentials which lead to similar predictions for thermodynamic data do not always predict similar microscopic mechanisms.

References

Allen, M.P., Tildesley, D.J.: Computer Simulation of Liquids. Clarendon, Oxford (1987)

Baerlocher, Ch., Meier, W.M., Olson, D.H.: Atlas of Zeolite Framework Types, 5th edn. Elsevier, Amsterdam (2001)

Beauvais, C., Guerrault, X., Coudert, F.X., Boutin, A., Fuchs, A.H.: Distribution of sodium cations in Faujasite-type-zeolite: a canonical parallel tempering simulation study. J. Phys. Chem. B **108**, 399–404 (2004)

Beauvais, C., Boutin, A., Fuchs, A.H.: Adsorption of water in zeolite sodium-faujasite. A molecular simulation study. C. R. Chim. **8**, 485–490 (2005)

Blake, N.P., Weakliem, P.C., Metiu, H.: Ab-initio-based transferable potential for sodalites. J. Phys. Chem. B **102**, 67–74 (1998)

Boddenberg, B., Rakhmatkariev, G.U., Hufnagel, S., Salimov, Z.: A calorimetric and statistical mechanics study of water adsorption in zeolite NaY. Phys. Chem. Chem. Phys. **4**, 4172–4180 (2002)

Buttefey, S., Boutin, A., Mellot-Draznieks, C., Fuchs, A.: A simple model for predicting the Na^+ distribution in anhydrous NaY and NaX zeolites. J. Phys. Chem. B **105**, 9569–9575 (2001)

Calero, S., Dubbledam, D., Krichna, R., Smit, B., Vlugt, T.J.H., Denayer, J.F.M., Martens, J.A., Maesen, T.L.M.: Understanding the role of sodium during adsorption: a force field for alkanes in sodium-exchanged Faujasite. J. Am. Chem. Soc. **126**, 11377–11386 (2004)

Corma, A.: From microporous to mesoporous molecular sieve materials and their use in catalysis. Chem. Rev. **97**, 2373–2420 (1997)

Dang, L.X.: Mechanism and thermodynamics of ion selectivity in aqueous solutions of 18-crown-6 ether: a molecular dynamics study. J. Am. Chem. Soc. **117**, 6954–6960 (1995)

Demontis, P., Suffritti, G.B.: Structure and dynamics of zeolites investigated by molecular dynamics. Chem. Rev. **97**, 2845–2878 (1997)

Devautour, S., Abdoulaye, A., Giuntini, J.C., Henn, F.: Localization of water molecules and sodium ions in Na-mordenite, by thermally stimulated current measurement. J. Phys. Chem. B **105**, 9297–9301 (2001)

Di Lella, A., Desbiens, N., Boutin, A., Demachy, I., Ungerer, P., Bellat, J.P., Fuchs, A.H.: Molecular simulation studies of water physisorption in zeolites. Phys. Chem. Chem. Phys. **8**, 5396–5406 (2006)

Fitch, A.N., Jobic, H., Renouprez, A.: Localization of benzene in sodium-Y zeolite by powder neutron-diffraction. J. Phys. Chem. **90**, 1311–1318 (1986)

Frenkel, D., Smit, B.: Understanding Molecular Simulation: From Algorithms to Applications, 2nd edn. Academic Press, London (2002)

Gedeon, A., Ito, T., Fraissard, J.: Study of the H_2O/NaY system: an example of the application of ^{129}Xe n.m.r. of the xenon probe to the investigation of the location of adsorbed phases. Zeolite **8**, 376–380 (1988)

Hu, K.-N., Hwang, L.-P.: The influence of adsorbed molecules on Na-sites in NaY zeolite investigated by triple-quantum ^{23}Na MAS NMR spectroscopy. Solid State Nucl. Magn. Reson. **12**, 211–220 (1998)

Jaramillo, E., Auerbach, S.M.: New force field for Na cations in faujasite-type zeolites. J. Phys. Chem. B **103**, 9589–9594 (1999)

Jiràk, Z., Vratislav, S., Bosàcek, V.: A neutron-diffraction study of H,Na-Y Zeolites. J. Phys. Chem. Solids **41**, 1089–1095 (1980)

Jorgensen, W.L., Jenson, C.: Temperature dependence of TIP3P, SPC, and TIP4P water from NPT Monte Carlo simulations: seeking temperatures of maximum density. J. Comp. Chem. **19**, 1179–1186 (1998)

Jorgensen, W.L., Chandrasekhar, J., Madura, J.D., Impey, R.W., Klein, M.L.: Comparison of simple potential functions for simulating liquid water. J. Chem. Phys. **79**, 926–935 (1983)

Karger, J., Vasenkov, S., Auerbach, S.M.: In: Auerbach, S.M., Carrado, K.A., Dutta, P.K. (eds.) Handbook of Zeolite Science and Technology. Dekker, New York (2003)

Kramer, G.J., Farragher, N.P., van Beest, B.W.H., van Santen, R.A.: Interatomic force-fields for silicas,aluminophosphates, and zeolites—derivation based on *ab-initio* calculations. Phys. Rev. B **43**, 5068–5080 (1991)

Loewenstein, W.: The distribution of aluminium in the tetrahedra of silicates and aluminates. Am. Mineral. **39**, 92–96 (1954)

Maurin, G., Bell, R.G., Devautour, S., Henn, F., Giuntini, J.C.: Modelling the effect of hydration in zeolite Na^+Mordenite. J. Phys. Chem. **108**, 3739–3745 (2004)

Maurin, G., Llewellyn, P.L., Poyet, Th., Kuchta, B.: Influence of extra-framework cations on the adsorption properties of X-Faujasite systems: microcalorimetry and molecular simulation. J. Phys. Chem. B **109**, 125–129 (2005)

Mellot, C.F., Ph.D. Thesis, Université Pierre et Marie Curie (1993)

Mellot-Draznieks, C., Buttefey, S., Boutin, A., Fuchs, A.H.: Placement of cations in NaX faujasite-type zeolite using (N, V, T) Monte Carlo simulations. Chem. Commun. **21**, 2200–2201 (2001)

Meunier, F.: In: Kanaeko, K., Kanoh, H., Hanzawa, Y. (eds.) Proceedings of the 7th Conference of Fundamentals of Adsorption, IK International (2001)

Meier, W., Olson, M.D.H.: Atlas of zeolite structures. In: Structure Commission of the International Zeolite Association. Elsevier, Amsterdam (1978)

Moïse, J.C., Bellat, J.P., Méthivier, A.: Adsorption of water vapor on X and Y zeolites exchanged with barium. Microporous Mesoporous Mater. **43**, 91–101 (2001)

Nicholson, D., Parsonage, N.G.: Computer Simulation and the Statistical Mechanics of Adsorption. Academic Press, New York (1982)

Nicolas, A., Devautour-Vinot, S., Maurin, G., Giuntini, J.C., Henn, F.: Location and de-trapping energy of sodium ions in dehydrated X

and Y faujasites determined by dielectric relaxation spectroscopy. Microporous Mesoporous Mater. **109**, 41–419 (2008a)

Nicolas, A., Devautour-Vinot, S., Maurin, G., Giuntini, J.C., Henn, F.: Unpublished results (2008b)

Olson, D.H.: The crystal-structure of dehydrated NaX. Zeolites **15**, 439–443 (1995)

Paulin, C., Bellat, J.P.: Unpublished results (2008)

Plant, D.F., Maurin, G., Jobic, H., Llewellyn, P.L.: Molecular dynamics simulation of the cation motion upon adsorption of CO_2 in faujasite zeolite systems. J. Phys. Chem. B **110**, 14372–14378 (2006)

Porcher, F., Souhassou, M., Dusausoy, Y., Lecomte, C.: The crystal structure of a low-silica dehydrated NaX zeolite. Eur. J. Mineral. **11**, 333–343 (1999)

Ramsahye, N.A., Bell, R.G.: Cation mobility and the sorption of chloroform in zeolite NaY: Molecular dynamics study. J. Phys. Chem. B **109**, 4738–4747 (2005)

Smit, B., Krishna, R.: Molecular simulation in zeolitic process design. Chem. Eng. Sci. **58**, 557–568 (2003)

Soler-Illia, G.J.D., Sanchez, C., Lebeau, B., Patarin, J.: Chemical strategies to design textured materials: From microporous and mesoporous oxides to nanonetworks and hierarchical structures. Chem. Rev. **102**, 4093–4138 (2002)

Tuñon, I., Martins-Costa, M.T.C., Millot, C., Ruiz-López, M.F.: Coupled density functional/molecular mechanics Monte Carlo simulations of ions in water. The bromide ion. Chem. Phys. Lett. **241**, 450–456 (1995)

Uytterhoeven, L., Dompas, D., Mortier, W.J.: Theoretical investigations on the interaction of benzene with faujasite. J. Chem. Soc. Faraday Trans. **88**, 2753–2760 (1992)

Vitale, G., Mellot, C.F., Bull, L.M., Cheetham, A.K.: Neutron diffraction and computational study of zeolite NaX: Influence of SIII′ cations on its complex with benzene. J. Phys. Chem. **101**, 4559–4564 (1997)

Zhu, L., Seff, K.J.: The crystal structure of a low-silica dehydrated NaX zeolite x. J. Phys. Chem. B **103**, 9512–9518 (1999)